Characterisation of Al0.52In0.48P mesa p-i-n photodiodes for X-ray photon counting spectroscopy

Article (Published Version)

AIP | Journal of Applied Physics

Characterisation of Al0.52In0.48P mesa p-i-n photodiodes for X-ray photon counting spectroscopy

S. Butera, G. Lioliou, A. B. Krysa, and A. M. Barnett

Citation: Journal of Applied Physics **120**, 024502 (2016); doi: 10.1063/1.4956153
View online: http://dx.doi.org/10.1063/1.4956153
View Table of Contents: http://scitation.aip.org/content/aip/journal/jap/120/2?ver=pdfcov
Published by the AIP Publishing

Characterisation of $Al_{0.52}In_{0.48}P$ mesa p-i-n photodiodes for X-ray photon counting spectroscopy

S. Butera,[1,a)] G. Lioliou,[1] A. B. Krysa,[2] and A. M. Barnett[1]
[1]*Semiconductor Materials and Device Laboratory, School of Engineering and Informatics, University of Sussex, Brighton BN1 9QT, United Kingdom*
[2]*EPSRC National Centre for III-V Technologies, University of Sheffield, Mappin Street, Sheffield S1 3JD, United Kingdom*

(Received 15 March 2016; accepted 25 June 2016; published online 12 July 2016)

Results characterising the performance of thin (2 μm i-layer) $Al_{0.52}In_{0.48}P$ p^+-i-n^+ mesa photodiodes for X-ray photon counting spectroscopy are reported at room temperature. Two 200 μm diameter and two 400 μm diameter $Al_{0.52}In_{0.48}P$ p^+-i-n^+ mesa photodiodes were studied. Dark current results as a function of applied reverse bias are shown; dark current densities <3 nA/cm^2 were observed at 30 V (150 kV/cm) for all the devices analysed. Capacitance measurements as a function of applied reverse bias are also reported. X-ray spectra were collected using 10 μs shaping time, with the device illuminated by an ^{55}Fe radioisotope X-ray source. Experimental results showed that the best energy resolution (FWHM) achieved at 5.9 keV was 930 eV for the 200 μm $Al_{0.52}In_{0.48}P$ diameter devices, when reverse biased at 15 V. System noise analysis was also carried out, and the different noise contributions were computed. *Published by AIP Publishing.* [http://dx.doi.org/10.1063/1.4956153]

I. INTRODUCTION

Wide bandgap photodetectors may play a very important role in aerospace and military applications; since they present lower leakage currents[1,2] than alternative narrower bandgap materials, such as silicon or germanium, they can operate at room temperature and above without cooling system.[3,4] Consequently, they potentially offer cheaper and more compact technologies that may be useful in space missions[5] and terrestrial applications outside the laboratory environment[6] requiring X-ray spectroscopy. X-ray photon counting spectroscopy has been demonstrated using different wide bandgap semiconductors: high-resolution X-ray spectra have already been achieved, even at high temperature, using SiC, GaAs, and AlGaAs detectors. Bertuccio *et al.*[3] reported X-ray spectroscopy, over the temperature range of 30 °C–100 °C, using a SiC X-ray detector. Energy resolutions (FWHM) at 5.9 keV of 196 eV and 233 eV were observed at 30 °C and 100 °C, respectively. Another material that can be used in X-ray spectroscopy is GaAs. Barnett *et al.* demonstrated 2 μm thick GaAs p^+-i-n^+ mesa X-ray photodiodes, at temperatures from −30 °C to 80 °C, with energy resolutions at 5.9 keV of 800 eV and 1.5 keV at 20 °C and 80 °C, respectively,[4] while Lioliou *et al.* reported 7 μm thick GaAs p^+-i-n^+ mesa X-ray photodiodes with energy resolutions at 5.9 keV of 750 eV at 20 °C.[2] At 23 °C, an energy resolution as low as 266 eV was achieved using GaAs detectors by Owens *et al.*[7] $Al_{0.8}Ga_{0.2}As$ photodiodes have also been demonstrated by Barnett *et al.*[8] to operate as photon counting spectroscopy X-ray detectors over the temperature ranges −30 °C to 90 °C; energy resolutions at 5.9 keV of 1.07 keV and 2.2 keV were observed at room temperature and at 90 °C, respectively, limited by the noise of the preamplifier used.

Another material usually used to produce efficient detection systems for soft and hard X-rays, as well as γ-rays, is CdTe.[9] CdTe and its related compounds (e.g., CdZnTe, CdMnTe) can be used for radiation detection at different temperatures. At −60 °C, energy resolutions (FWHM) of 310 eV and 600 eV at 5.9 keV and 59 keV, respectively, were reported using CdTe detector;[10] at −37 °C, FWHM of 311 eV and 824 eV at 5.9 keV and 59 keV, respectively, were demonstrated for a CdZnTe detector.[11] These compounds can also operate at increased temperatures, albeit with degraded energy resolution: for example, 53 keV (FWHM) at 122 keV was observed for CdTe at 92 °C,[12] whilst a 9.4 keV (FWHM) at 32 keV was reported for CdZnTe at 70 °C.[13] CdTe and CdZnTe are attractive choices for producing large area radiation detectors, and for this reason, they have received considerable research attention;[14] spectroscopic CdZnTe and CdTe detector imaging arrays, for example, have been proven by Wilson *et al.*[15]

A III-V wide bandgap ternary compound that could be very useful for radiation detection at high temperatures is $Al_{0.52}In_{0.48}P$.[16] $Al_{0.52}In_{0.48}P$ can be beneficial in many applications (e.g., space missions) since it allows the detection of wide range of X-ray energies: AlInP structures, with an appropriate thick charge collection layer, can be used to detect hard X-rays as well as soft X-ray photons. The use of $Al_{0.52}In_{0.48}P$ for X-ray spectroscopy is a new research field that can provide innovative X-ray systems with high-energy resolution.[17] $Al_{0.52}In_{0.48}P$ has an indirect bandgap of 2.31 eV,[18] and it is nearly lattice matched with GaAs. $Al_{0.52}In_{0.48}P$ is widely used in semiconductor optoelectronics, and the crystalline quality of the nearly lattice matched $Al_{0.52}In_{0.48}P$ can be very high in comparison to III-V nitrides, IV, and II-VI compounds of a similar bandgap. The doping in $Al_{0.52}In_{0.48}P$ is also easier to control than in some II-VI semiconductors. This paper reports initial characterisation of $Al_{0.52}In_{0.48}P$ p^+-i-n^+ mesa

a)Author to whom correspondence should be addressed. Electronic mail: S.Butera@sussex.ac.uk.

photodiodes for X-ray photon counting spectroscopy. For the first time, a non-avalanche $Al_{0.52}In_{0.48}P$ photodiode was used in a spectrometer and a system energy resolution of 930 eV at 5.9 keV for a 200 μm device observed; these significant results have been achieved because of the high performances of the $Al_{0.52}In_{0.48}P$ detector used and the custom low-noise charge sensitive preamplifier electronics developed at our laboratory. The $Al_{0.52}In_{0.48}P$ device is the thickest i-layer mesa $Al_{0.52}In_{0.48}P$ detector produced so far, highlighting the advanced growth and fabrication technologies used.

II. DEVICE STRUCTURE

The $Al_{0.52}In_{0.48}P$ epilayer of the device was grown by metalorganic vapour phase epitaxy (MOVPE) on a commercial (100) n-GaAs: Si substrate with a misorientation of 10° towards ⟨111⟩A to suppress the CuPt-like ordered phase. The doping concentrations of the $Al_{0.52}In_{0.48}P$ p and n layers were $5 \times 10^{17}\,cm^{-3}$ and $2 \times 10^{18}\,cm^{-3}$, respectively. The layers' thicknesses were 0.2 μm for the p^+-region, 2 μm for the i-region, and 0.1 μm for the n^+-region. After growth, the wafer was processed to form mesa structures using 1:1:1 H_3PO_4:H_2O_2:H_2O solution followed by 10 s in 1:8:80 H_2SO_4:H_2O_2:H_2O solution. Unpassivated 200 μm and 400 μm diameter $Al_{0.52}In_{0.48}P$ mesa photodiodes were produced. An Ohmic rear contact consisting of 20 nm of InGe and 200 nm of Au was evaporated onto the rear of the substrate and an Ohmic top contact consisting of 20 nm of Ti and 200 nm of Au was evaporated on the p-side of the mesa device. The top Ohmic contact had an annular shape; it covered 33% and 45% of the surface of the 400 μm and 200 μm diameter photodiodes, respectively. The device layers, their relative thicknesses, and materials are summarised in Table I.

Using the Beer-Lambert law and assuming complete charge collection in the p-, i-, and n-layers, X-ray quantum efficiencies (*QEs*) through the device optical window (region not covered by contacts) were calculated as a function of photon energy up to 10 keV for the $Al_{0.52}In_{0.48}P$ p^+-i-n^+ mesa photodiodes (Fig. 1).

X-ray quantum efficiencies (*QEs*) of 22% and 18% were calculated for the device for 5.9 keV and 6.49 keV photons, respectively. The $Al_{0.52}In_{0.48}P$ attenuation coefficients at 5.9 keV and 6.49 keV were estimated[19,20] to be 0.1109 μm^{-1} and 0.0856 μm^{-1}. The attenuation coefficients at 5.9 keV and 6.49 keV in $Al_{0.52}In_{0.48}P$ are higher than GaAs (0.0837 μm^{-1} and 0.0645 μm^{-1}, respectively[19]), Si (0.0346 μm^{-1} and 0.0263 μm^{-1}, respectively[21]), and $Al_{0.8}Ga_{0.2}As$ (0.0788 μm^{-1} and 0.0604 μm^{-1}, respectively[20]).

TABLE I. Layer details of the $Al_{0.52}In_{0.48}P$ photodiode.

Layer	Material	Thickness (μm)	Dopant	Dopant type	Doping density (cm^{-3})
1	Ti	0.02			
2	Au	0.2			
3	GaAs	0.01	Zn	p^+	1×10^{19}
4	$Al_{0.52}In_{0.48}P$	0.2	Zn	p^+	5×10^{17}
5	$Al_{0.52}In_{0.48}P$	2	Undoped		
6	$Al_{0.52}In_{0.48}P$	0.1	Si	n^+	2×10^{18}
7	Substrate n^+ GaAs				
8	Au	0.2			
9	InGe	0.02			

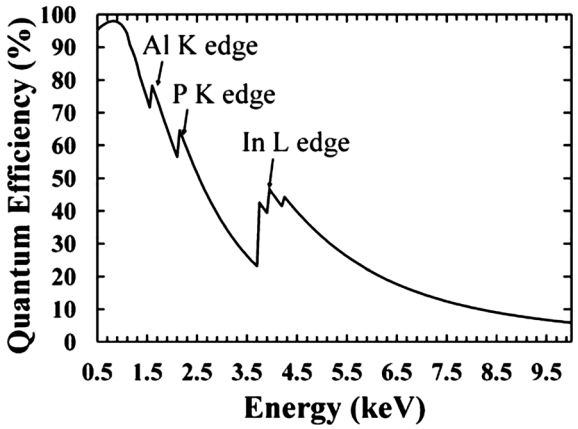

FIG. 1. Calculated quantum efficiency of $Al_{0.52}In_{0.48}P$ p^+-i-n^+ mesa photodiodes as a function of photon energy. The discontinuities shown correspond to the aluminium and phosphorus K X-ray edges and indium L X-ray edge.

III. EXPERIMENTAL RESULTS

A. Electrical characterisation: Current-voltage and capacitance-voltage measurements

Two 200 μm diameter (D1 and D2) and two 400 μm diameter (D3 and D4) $Al_{0.52}In_{0.48}P$ photodiodes were investigated at room temperature in a dry nitrogen atmosphere (relative humidity $< 5\%$). The devices studied were randomly selected from those available and were unpassivated.

Dark current characteristics as functions of applied bias were measured. Reverse bias measurements from 0 V to 30 V were made in 1 V increments using a computer controlled Keithley 6487 picoammeter/voltage source. The uncertainty associated with the current readings was 0.3% of their values plus 400 fA, while the uncertainty associated with the applied biases was 0.1% of their values plus 1 mV.[22] Dark current densities $<3\,nA/cm^2$ were observed at 30 V (150 kV/cm) for all the devices analysed. These values are comparable with previously reported high quality $Al_{0.52}In_{0.48}P$ p^+-i-n^+ photodiodes having 1.03 μm i-layer thickness.[23] The reported leakage current was lower than GaAs ($1.08\,nA/cm^2$ at 22 kV/cm)[2] and $Al_{0.8}Ga_{0.2}As$ ($4.72\,nA/cm^2$ at 29 kV/cm)[24] detectors at similar electric fields and temperatures. The $Al_{0.52}In_{0.48}P$ dark current density was greater than for some previously reported SiC detectors ($\sim 1\,pA/cm^2$ at 103 kV/cm)[3] at similar electric field and temperatures. Fig. 2 shows the dark current density as a function of reverse bias for the presently reported $Al_{0.52}In_{0.48}P$ photodiodes. The different sized devices had different leakage current density, indicating that surface leakage current was significant in the analysed photodiodes. In a mesa photodiode, the dark current consists of a bulk leakage contribution, which is proportional to the mesa area, and the surface leakage contribution, which is proportional to the mesa perimeter.[25,26] If the surface leakage current is negligible, the current density for different sized devices should be constant;

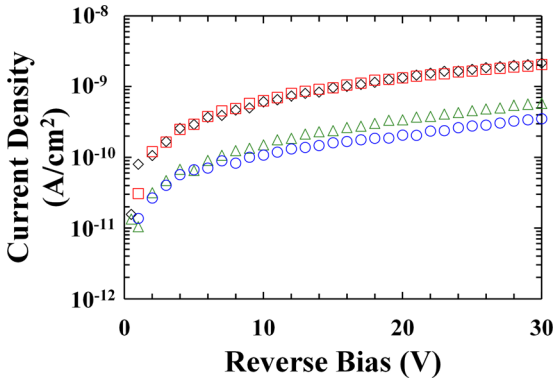

FIG. 2. Dark current density as a function of applied reverse bias at room temperature for $Al_{0.52}In_{0.48}P$ devices. Empty rhombuses (black) and empty squares (red) referred to the data taken on the two 200 μm diameter devices, D1 and D2, respectively; empty circles (blue) and empty triangles (green) referred to the data taken on the two 400 μm diameter devices, D3 and D4, respectively.

consequently, if current densities do not match across diodes of different size, this means that the surface contribution is significant.

The depletion depths and the doping concentrations in the intrinsic regions of the devices were calculated from capacitance measurements at room temperature. The capacitance was measured as a function of applied reverse bias, between 0 V and 20 V, using an HP 4275 A Multi Frequency LCR meter. The test signal was sinusoidal with a 50 mV rms magnitude and 1 MHz frequency. The capacitance of an identical empty package was also measured, 0.77 pF $\pm$ 0.02 pF, and subtracted from the measured capacitance of the packaged photodiodes to determine the capacitance of the devices themselves. The uncertainty associated with each capacitance reading was ~0.12%,[27] while the uncertainty associated with the applied biases was 0.1% of their values plus 1 mV. Figs. 3(a) and 3(b) show the capacitance as a function of applied reverse bias for the 200 μm and 400 μm diameter devices, respectively. The variations in the capacitance values between diodes of same diameters were within the experimental repeatability accuracy ($\pm$0.03 pF).

For each diode analysed, the depletion depth (W) was calculated by

$$W = \frac{\varepsilon_0 \varepsilon_r A}{C}, \tag{1}$$

where ε_0 is the permittivity of the vacuum, ε_r is the $Al_{0.52}In_{0.48}P$ dielectric constant (11.25[23]), and A is the device area.[28]

Figs. 4(a) and 4(b) show the depletion depth as a function of applied reverse bias for the 200 μm and 400 μm diameter devices, respectively.

The application of the reverse bias to the diode increased the depth of the depletion region. At reverse bias bigger than 5 V, the depletion region approached the n-layer and increased more slowly due to the higher doping concentration in the doped regions. The measured discrepancy in depletion depth at 20 V between the 200 μm and 400 μm devices was smaller than its uncertainty, which was calculated to be (0.08 $\pm$ 0.17) μm.

The doping concentration, N, at a certain depletion depth, W, was determined by

$$N(W) = \frac{2}{q\varepsilon_0\varepsilon_r A^2}\left(\frac{dV}{d\left[\frac{1}{C^2}\right]}\right), \tag{2}$$

where ε_0 is the permittivity of the vacuum, ε_r is the $Al_{0.52}In_{0.48}P$ dielectric constant (11.25[23]), and A is the device area.[28] Fig. 5 is an example of the determined doping carrier concentration calculated as a function of depletion depth; in this particular case, the results from one of the

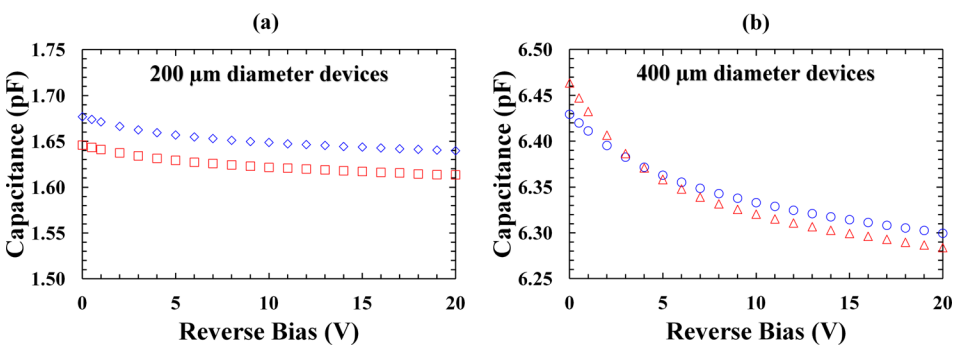

FIG. 3. Capacitance as a function of applied reverse bias at room temperature (a) for the 200 μm diameter $Al_{0.52}In_{0.48}P$ devices, D1 (blue empty rhombuses) and D2 (red empty squares), and (b) for the 400 μm diameter $Al_{0.52}In_{0.48}P$ devices, D3 (blue empty circles) and D4 (red empty triangles).

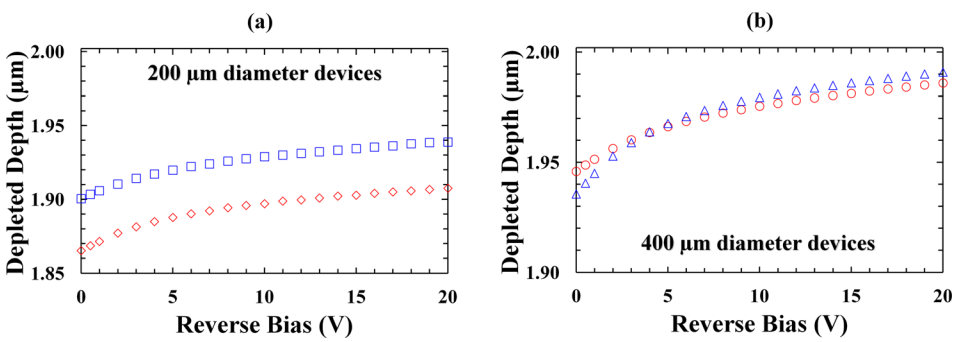

FIG. 4. Depletion depth as a function of applied reverse bias at room temperature (a) for the 200 μm diameter $Al_{0.52}In_{0.48}P$ devices, D1 (red empty rhombuses) and D2 (blue empty squares), and (b) for the 400 μm diameter $Al_{0.52}In_{0.48}P$ devices, D3 (red empty circles) and D4 (blue empty triangles).

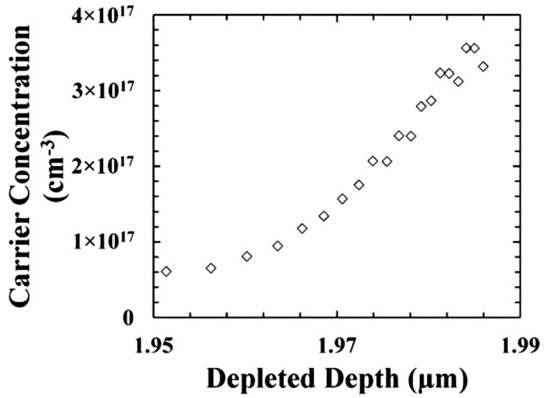

FIG. 5. Doping concentration below the p^+-i junction as a function of depletion depth at room temperature for 400 μm diameter $Al_{0.52}In_{0.48}P$ device (D3).

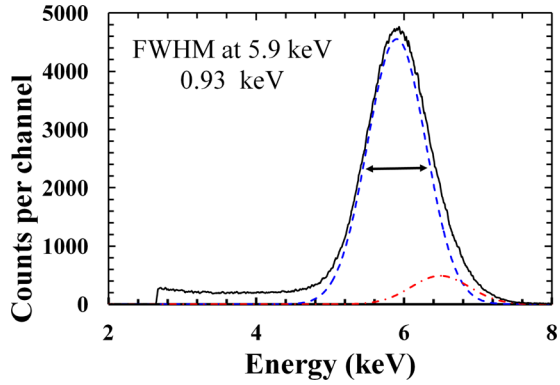

FIG. 6. ^{55}Fe X-ray spectrum accumulated at 15 V reverse bias using 200 μm diameter $Al_{0.52}In_{0.48}P$ device (D2) at room temperature. The shaping time used is 10 μs. Also shown are the fitted Mn Kα (blue dashed line) and Mn Kβ (red dashed-dotted line) peaks.

400 μm diameter devices are presented. Similar results, as expected, were obtained for the other samples characterised. The doping density in the i-layer was found to be $(4.3 \pm 0.7) \times 10^{16}\,cm^{-3}$; this value increased to $(3.5 \pm 0.4) \times 10^{17}\,cm^{-3}$ at i-n interface.

B. X-ray spectroscopy and noise analysis

At different applied biases, X-ray spectra were collected using the 200 μm and 400 μm diameter devices. An ^{55}Fe radioisotope X-ray source (Mn Kα = 5.9 keV, Mn Kβ = 6.49 keV) was positioned 5 mm above the top of the $Al_{0.52}In_{0.48}P$ mesa photodiodes. Each diode in turn was connected to a custom-made, single channel, charge sensitive preamplifier of feedback resistorless design.[29] The output from the preamplifier was connected to an Ortec 572A shaping amplifier and then to a multichannel analyser (MCA). The shaping time was 10 μs, and the live time limit for each accumulated spectrum was 1000 s. The experiment was performed at room temperature in a dry nitrogen atmosphere (relative humidity <5%). Spectra were accumulated with each diode reverse biased at 0 V, 5 V, 10 V, and 15 V. As the applied reverse bias was increased, an improvement in energy resolution (as quantified by the FWHM at 5.9 keV) was observed; this was attributed to less charge trapping noise at greater electric field strengths as the effects of reduced capacitance were negligible. Fig. 6 shows an X-ray spectrum obtained at 15 V using a 200 μm diameter device. The counts of the zero energy noise peak of the preamplifier were limited by setting the MCA's low energy threshold to appropriate energy cut-off values (2.67 keV) after the position of the zero energy peak had been established. The ^{55}Fe photopeak observed was the combination of the Mn Kα and Mn Kβ lines at 5.9 keV and 6.49 keV, respectively. In Fig. 6, the fitted Gaussians representing the Mn Kα and Mn Kβ peaks are shown: the fittings took into account the relative X-ray emission rates of the ^{55}Fe radioisotope X-ray source at 5.9 keV and 6.49 keV in the appropriate ratio[30] and the relative difference in efficiency of the detector at these X-ray energies.

An energy resolution (FWHM) at 5.9 keV of 930 eV was measured for both the 200 μm diameter $Al_{0.52}In_{0.48}P$ devices studied. The FWHM at 5.9 keV was 1.2 keV for both the 400 μm diameter $Al_{0.52}In_{0.48}P$ devices.

The energy resolution (FWHM) of non-avalanche X-ray photodiode spectrometers is broadened by three classes of noise: Fano noise, charge trapping noise, and electronic noise.[31] The Fano noise is due to the statistical nature of the impact ionisation process. If the electron-hole pair creation energy (ω) in $Al_{0.52}In_{0.48}P$ was 5.8 eV (2.5 times the bandgap) and the Fano factor (F), using a conservative assumption, 0.12, the likely Fano noise was estimated to be 151 eV FWHM at 5.9 keV. It should be noted that measurements of the electron-hole pair creation energy and the Fano factor are yet to be reported for $Al_{0.52}In_{0.48}P$. Knowledge of ω and F and their temperature dependences is important because they in part determine the statistically limited spectral resolution of an X-ray detector. The electronic noise consists of parallel white noise, series white noise, 1/f noise, and dielectric noise.[32,33] The parallel white noise takes into account the leakage currents of the detector and input junction field-effect transistor (JFET) of the preamplifier, whilst the series white noise takes into account the capacitances of the detector and input JFET of the preamplifier. The parallel white noise, series white noise, and 1/f noise were calculated for the reported detectors. The series white noise contribution was adjusted for induced gate current noise.[34] Each noise contribution was found to be similar for devices with same diameter. Fig. 7 shows the parallel white noise, series white noise, and 1/f noise values as a function of reverse bias for 200 μm diameter (a) and 400 μm diameter (b) devices.

At every applied reverse bias, the parallel white noise values were very similar between all the diodes under analysis; this was due to similar leakage currents (maximum 0.3 pA at 15 V). In both the 400 μm diameter devices, the series white noise and the 1/f noise values, instead, were bigger with respect to the 200 μm diameter devices, resulting in FWHM broadening at 5.9 keV; this was due to the higher device capacitance. Charge trapping noise is due to incomplete charge collection. The combined contribution of the dielectric noise and charge trapping noise at 5.9 keV was calculated by subtracting in quadrature the Fano noise, parallel white noise, series white noise, and 1/f noise contributions at

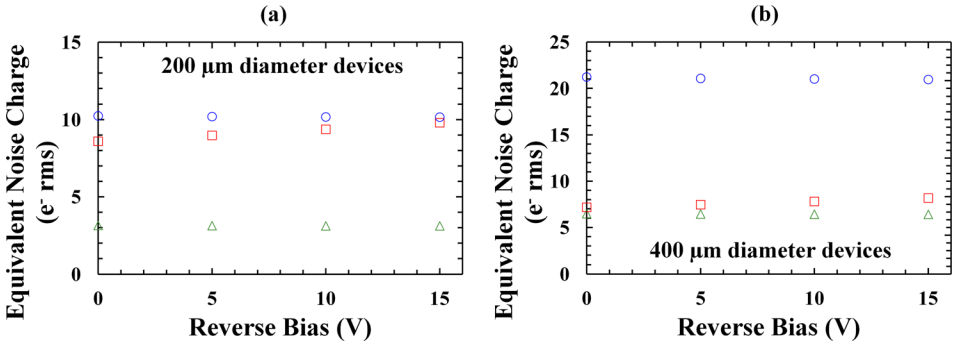

FIG. 7. Equivalent noise charge as a function of applied reverse bias at room temperature using (a) 200 μm diameter $Al_{0.52}In_{0.48}P$ device, D1, and (b) 400 μm diameter device D3. In both graphs, the parallel white noise (red empty squares), the series white noise (blue empty circles), and the 1/*f* noise (green empty triangles) contributions are shown.

5.9 keV from the measured FWHM at 5.9 keV. The computed combined dielectric and trapping noise contributions at 5.9 keV are reported in Fig. 8.

For all the photodiodes analysed, the dielectric and trapping noise contribution at 5.9 keV is bigger at 0 V than at higher voltages. This is due to the great trapping noise at 0 V. At an increased reverse bias, the charge transport improved resulting in less trapping noise. Since the dielectric noise is expected to be independent of reverse bias,[31] the reduction in equivalent noise charge (ENC) shown in Fig. 8 can be attributed to reductions in charge trapping noise as a consequence of improved charge transport at higher electric fields. For the 200 μm and 400 μm diameter diodes, when the reverse bias was increased from 10 V to 15 V, the charge trapping noise was reduced by 18 e^- rms ENC and 34 e^- rms ENC, respectively. These contributions were small compared with the other noise sources.

At room temperature, the spectral resolutions at 5.9 keV reported here for $Al_{0.52}In_{0.48}P$ photodiodes are worse than the spectral resolutions at 5.9 keV observed by Bertuccio *et al.*[3] for SiC detectors (196 eV) and Owens *et al.*[7] for GaAs detectors (266 eV); largely, this can be attributed to the lower electronic noise associated with their device' readout electronics and also the extremely high quality materials used. In the presently reported $Al_{0.52}In_{0.48}P$ study, device readout electronics similar to Lioliou *et al.*[2] and Barnett *et al.*[8] were used. The energy resolutions achieved with the present $Al_{0.52}In_{0.48}P$ detectors are slightly poorer than those reported with GaAs (750 eV) by Lioliou *et al.*,[2] but better than those reported with $Al_{0.8}Ga_{0.2}As$ (1.07 eV) by Barnett *et al.* for $Al_{0.8}Ga_{0.2}As$.[8] $Al_{0.52}In_{0.48}P$ detectors are performing better than $Al_{0.8}Ga_{0.2}As$ detectors at room temperature; this is interesting since the optimum bandgap for the room temperature operation (1.5 eV (Refs. 35 and 36)) is closer to the $Al_{0.8}Ga_{0.2}As$ bandgap (2.09 eV) than that of $Al_{0.52}In_{0.48}P$ (2.31 eV). This may be an indication of a lower than expected electron-hole pair creation energy in $Al_{0.52}In_{0.48}P$ or smaller charge trapping noises in $Al_{0.52}In_{0.48}P$.

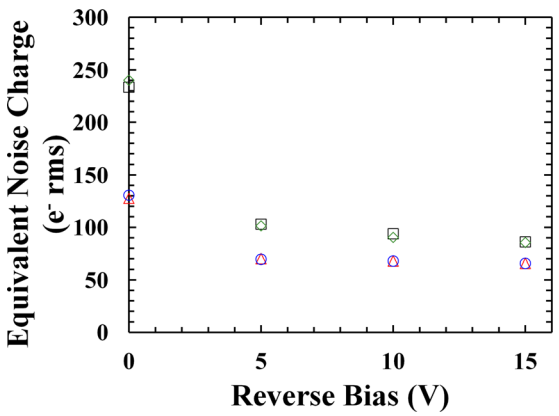

FIG. 8. Equivalent noise charge of the dielectric and trapping noise contribution at 5.9 keV as a function of applied reverse bias at room temperature. Empty circles (blue) and empty triangles (red) refer to the calculated dielectric and trapping noise at 5.9 keV on the two 200 μm diameter devices, D1 and D2, respectively; empty rhombuses (green) and empty squares (black) refer to the calculated dielectric and trapping noise at 5.9 keV of the two 400 μm diameter devices, D3 and D4, respectively.

IV. CONCLUSION

In this paper, results characterising prototype non-avalanche $Al_{0.52}In_{0.48}P$ p^+-i-n^+ mesa X-ray photodiodes were investigated as detectors for X-ray photon counting spectroscopy at room temperature using an ^{55}Fe radioisotope X-ray source. Initial dark current and capacitance measurements as functions of applied reverse bias are reported for 400 μm diameter and 200 μm diameter devices. Dark current densities <3 nA/cm^2 were observed at 30 V for all the $Al_{0.52}In_{0.48}P$ devices. At 0 V, capacitances of 6.5 pF and 1.7 pF were observed for the 400 μm diameter and 200 μm diameter devices, respectively. ^{55}Fe X-ray spectra were collected using the devices. The results showed that the best energy resolution at 5.9 keV, 930 eV FWHM, was achieved at a reverse bias of 15 V for the 200 μm diameter devices. The FWHM at 5.9 keV was 1.2 keV for both the 400 μm diameter $Al_{0.52}In_{0.48}P$ devices under the same conditions. System noise analyses showed that the series white and the 1/*f* noises were bigger in the 400 μm diameter devices with respect to the 200 μm diameter devices; this was due to the higher capacitance. The parallel white noise was also computed, and it was similar between all the diodes under analysis; this was due to similar leakage currents. The main source of noise limiting the energy resolution of the reported system was the combined contribution of the dielectric noise and charge trapping noise. At reverse biases >0 V, the charge transport improved, resulting in less trapping noise and corresponding better energy resolution.

ACKNOWLEDGMENTS

This work was supported by the STFC Grant Nos. ST/M002772/1 and ST/M004635/1 (University of Sussex, A.M.B., PI) and the Royal Society Grant RS130515 (University of

Sussex, A.M.B., PI). The authors are grateful to R. J. Airey and S. Kumar at the EPSRC National Centre for III-V Technologies for device fabrication. G. Lioliou acknowledges the funding received from the University of Sussex in the form of a Ph.D. scholarship.

Authors' Data Statement: Data underlying this work are subject to commercially confidentiality. The Authors regret that they cannot grant public requests for further access to any data produced during the study.

[1]G. Lioliou, M. Mazzillo, A. Sciuto, and A. M. Barnett, Opt. Express **23**, 21657 (2015).
[2]G. Lioliou, X. Meng, J. S. Ng, and A. M. Barnett, Nucl. Instrum. Methods Phys. Res., Sect. A **813**, 1 (2016).
[3]G. Bertuccio, S. Caccia, D. Puglisi, and D. Macera, Nucl. Instrum. Methods Phys. Res., Sect. A **652**, 193 (2011).
[4]A. M. Barnett, J. E. Lees, D. J. Bassford, J. S. Ng, C. H. Tan, N. Babazadeh, and R. B. Gomes, Nucl. Instrum. Methods Phys. Res., Sect. A **654**, 336 (2011).
[5]J. L. Barth, C. S. Dyer, and E. G. Stassinopoulos, IEEE Trans. Nucl. Sci. **50**, 466 (2003).
[6]D. M. Kocak, F. R. Dalgleish, F. M. Caimi, and Y. Y. Schechner, Mar. Technol. Soc. J. **42**, 52 (2008).
[7]A. Owens, M. Bavdaz, A. Peacock, A. Poelaert, H. Andersson, S. Nenonen, L. Troger, and G. Bertuccio, Nucl. Instrum. Methods Phys. Res., Sect. A **466**, 168 (2001).
[8]A. M. Barnett, D. J. Bassford, J. E. Lees, J. S. Ng, C. H. Tan, and J. P. R. David, Nucl. Instrum. Methods Phys. Res., Sect. A **621**, 453 (2010).
[9]A. Owens and A. Peacock, Nucl. Instrum. Methods Phys. Res., Sect. A **531**, 18 (2004).
[10]A. Loupilov, A. Sokolov, and V. Gostilo, J. Radiat. Phys. Chem. **61**, 463 (2001).
[11]A. Owens, M. Bavdaz, H. Andersson, T. Gagliardi, M. Krumrey, S. Nenonen, A. Peacock, and I. Taylor, Nucl. Instrum. Methods Phys. Res., Sect. A **484**, 242 (2002).
[12]M. R. Squillante and G. Entine Nucl. Instrum. Methods Phys. Res., Sect. A **380**, 160 (1996).
[13]S. U. Egarievwe, K. T. Chen, A. Burger, R. B. James, and C. M. Lisse, J. X-Ray Sci. Technol. **6**, 309 (1996).
[14]P. J. Sellin, Nucl. Instrum. Methods Phys. Res., Sect. A **563**, 1 (2006).
[15]M. D. Wilson, S. J. Bell, R. J. Cernik, C. Christodoulou, C. K. Egan, D. O'Flynn, S. Jacques, S. Pani, J. Scuffham, P. Seller, P. J. Sellin, R. Speller, and M. C. Veale, IEEE Trans. Nucl. Sci. **60**, 1197 (2013).
[16]Y. G. Zhang, C. Li, Y. Gu, K. Wang, H. Li, X. M. Shao, and J. X. Fang, IEEE Photonics Technol. Lett. **22**, 944 (2010).
[17]A. Auckloo, J. S. Cheong, X. Meng, C. H. Tan, J. S. Ng, A. B. Krysa, R. C. Tozer, and J. P. R. David, J. Inst. **11**, P03021 (2016).
[18]J. S. Cheong, J. S. Ong, J. S. Ng, A. B. Krysa, and J. P. R. David, IEEE J. Sel. Top. Quantum Electron. **20**, 142 (2014).
[19]D. T. Cromer and D. Liberman, J. Chem. Phys. **53**, 1891 (1970).
[20]R. Jenkins, R. W. Gould, and D. Gedcke, *Quantitative X-Ray Spectrometry*, 2nd ed. (CRC Press, New York, 1995).
[21]J. H. Hubbell, Int. J. Appl. Radiat. Isot. **33**, 1269 (1982).
[22]Keithley Instruments, Inc., *Model 6487 Picoammeter/Voltage Source Reference Manual*, 6487-901-01 Rev B (Cleveland, 2011).
[23]J. S. L. Ong, J. S. Ng, A. B. Krysa, and J. P. R. David, IEEE Electron Device Lett. **32**, 1528 (2011).
[24]A. M. Barnett, G. Lioliou, and J. S. Ng, Nucl. Instrum. Methods Phys. Res., Sect. A **774**, 29 (2015).
[25]X. G. Zheng, J. S. Hsu, J. B. Hurst, X. Li, S. Wang, X. Sun, A. L. Holmes, J. C. Campbell, A. S. Huntington, and L. A. Coldren, IEEE J. Quantum Electron. **40**, 1068 (2004).
[26]P. J. Ker, A. R. J. Marshall, A. B. Krysa, J. P. R. David, and C. H. Tan, IEEE J. Quantum Electron. **47**, 1123 (2011).
[27]Hewlett Packard, *Model HP 4275A Multi-Frequency LCR Meter Manual*, 04275-90004 (Tokyo, 1990).
[28]S. M. Sze and K. K. Ng, *Physics of Semiconductor Devices*, 3rd ed. (John Wiley & Sons, New Jersey, 2007).
[29]G. Bertuccio, P. Rehak, and D. Xi, Nucl. Instrum. Methods Phys. Res., Sect. B **326**, 71 (1993).
[30]U. Shotzig, Appl. Radiat. Isot. **53**, 469 (2000).
[31]G. Lioliou and A. M. Barnett, Nucl. Instrum. Methods Phys. Res., Sect. A **801**, 63 (2015).
[32]G. A. Bertuccio, A. Pullia, and G. De Geronimo, Nucl. Instrum. Methods Phys. Res., Sect. A **380**, 301 (1996).
[33]E. Gatti, P. F. Manfredi, M. Sampietro, and V. Speziali, Nucl. Instrum. Methods Phys. Res., Sect. A **297**, 467 (1990).
[34]A. M. Barnett, J. E. Lees, D. J. Bassford, and J. S. Ng, Nucl. Instrum. Methods Phys. Res., Sect. A **673**, 10 (2012).
[35]G. A. Armantrout, S. P. Swierkowski, J. W. Sherohman, and J. H. Yee, IEEE Trans. Nucl. Sci. **24**, 121 (1977).
[36]S. P. Swierkowski and G. A. Armantrout, IEEE Trans. Nucl. Sci. **22**, 205 (1975).